J. Fluid Mech. (1989), *vol.* 209, *pp.* 359–384
Printed in Great Britain

Instability and filamentation of finite-amplitude waves on vortex layers of finite thickness

By D. I. PULLIN[1], P. A. JACOBS[1], R. H. J. GRIMSHAW[2] AND P. G. SAFFMAN[3]

[1] Department of Mechanical Engineering, The University of Queensland, St Lucia, QLD 4067, Australia

[2] School of Mathematics, The University of New South Wales, PO Box 1, Kensington, NSW, Australia

[3] Applied Mathematics, 217-50, Firestone Laboratory, California Institute of Technology, Pasadena, CA 91125, USA

(Received 4 July 1988 and in revised form 22 May 1989)

We study the instability of finite-amplitude waves on uniform vortex layers of finite thickness bounded by a plane rigid surface. A weakly nonlinear analysis of vorticity interface perturbations, and spectral stability calculations using the full equations of motion, together show that steady progressive waves are unstable to general subharmonic perturbations in the range $0.094 < d/\lambda < 1.7$, where d is the mean layer thickness and λ is the primary wavelength. The relevance of this instability to ultimate interface filamentation is tested by performing several numerical contour-dynamical simulations of the nonlinear interface evolution for initial disturbances consisting of the finite amplitude wave plus eigenfunctions obtained from the spectral calculations. The results indicate that within the band of unstable wavelengths, small perturbations to the steady non-uniform flow given by the finite amplitude wave motion (vortex equilibrium) are able to grow in magnitude, until at a time t_f, the wave extremum encounters a hyperbolic critical point of the velocity field after which filamentation occurs. Arguments are put forward based on the unsteady simulations with the purpose of identifying the preferred frame of reference for viewing the kinematical events controlling the filamentation process. An estimate for t_f is then made, and the mechanism of filamentation found is discussed in relation to the recently proposed nonlinear-cascade mechanism of Dritschel (1988*a*).

1. Introduction

The numerical technique of contour dynamics (CD) (see Deem & Zabusky 1978*a*, *b*; Zabusky, Hughes & Roberts 1979) has proved a powerful tool in the study of vortex mechanics for plane incompressible rotational flow of an inviscid fluid. Workers utilizing the CD method for the computation of vortex evolution problems have however, often encountered the onset of rapid distortions in the vorticity discontinuities (contours) with profound effects for both the vortex structure of the flow under study and also for the subsequent numerical integrity of the computations. These contour distortions have usually been characterized by the convective growth of either extrusive or intrusive filaments of fluid with one value of the vorticity into a body of fluid with a different numerical vorticity. This behaviour has become known as the 'filamentation' phenomenon, and despite recent progress towards its

analysis (e.g. Dritschel 1988*a*), a complete account of the mechanisms controlling filament generation has yet to emerge.

Applying the CD method to the Vlasov equation of plasma dynamics, Berk, Neilsen & Roberts (1970) noted the production of 'spray' in the numerical simulation of the phase-space hole–hole interaction problem (see also Roberts & Christiansen 1972). Deem & Zabusky (1978*a*, *b*) observed the ejection of extrusive vorticity filaments on a very small scale in CD calculations of isolated vortex patch dynamics. Pullin (1981) studied the evolution of large finite-amplitude disturbances with waveheight δ and wavelength λ, to a wall-bounded vortex layer of mean thickness d, finding intrusive filamentation when

$$\frac{\delta}{\lambda} \geqslant \frac{1}{4\pi}[1-\exp(-4\pi d/\lambda)]. \tag{1.1}$$

Filamentation was interpreted as the interaction of an extremum of the displaced vorticity discontinuity with the mean flow at the level of the (perturbed) critical layer. Equation (1.1) specifies an effective minimum amplitude of the disturbance at the onset of filamentation: note that in (1.1) amplitude is non-dimensionalized with respect to wavelength λ and not depth d, and hence is a measure of wave steepness. Results broadly consistent with (1.1) were found by Stern (1985) for isolated disturbances in an unbounded fluid with both barotropic flow and for flow with potential vorticity, and by Stern & Pratt (1985) in a study of vorticity front propagation in the presence of a wall.

Many of the previously cited papers considered the evolution of either initially (very) large disturbances to otherwise parallel shear flow, or of non-equilibrium initial configurations (e.g. Stern & Pratt 1985). The spatial resolution was usually low, and where filamentation was encountered, computations extended over only a few multiples of the characteristic flow timescale. Dritschel (1988*a*) (hereinafter referred to as D1) recognized that filamentation may result from the slow growth of disturbances with initially small waveheight to states of uniform vortex equilibria. Using a high resolution CD code based on 'contour surgery' (Dritschel 1988*b*), D1 obtained long timescale calculations of filamentation resulting from the propagation of either symmetrical or antisymmetrical isolated disturbances on the boundary of a uniform circular vortex. Arguments based on an analysis of the structure of a weakly nonlinear approximation to the full evolutionary CD equations were used to show that, provided disturbances do indeed grow in steepness, then they will do so at a rate proportional to the square of the initial steepness. Since this result holds for arbitrarily small initial steepness and since growth was found in each of several specific computations of both the weakly nonlinear and the full CD equations, D1 concluded that filamentation following growth in steepness will occur for almost all disturbances to vortex equilibria (of which the circular vortex is a specific example) of any steepness whatever. This appears to contradict conclusions drawn by Pullin (1981) and by Stern (1985), that a minimum amplitude is required.

In the present paper we discuss instability and filamentation of spatially periodic waves on vortex layers of finite thickness. We discuss cases for which the wave amplitude is either finite or arbitrarily small. Spectral calculations (§5) based on the direct computation of stability to generalized subharmonic disturbances and also results from the nonlinear Schrödinger equation in the long-wave, small-amplitude limit (§3) reveal instability of the finite-amplitude waves at arbitrarily small

amplitude and with growth rate proportional to the amplitude squared, over only a finite range of d/λ. In §6 we present the results of direct numerical integration of the full CD equations which suggest that this instability gives a mechanism for filamentation where, following slow growth of the wave amplitude, the disturbance extremum approaches a hyperbolic critical point of the velocity field at or near the critical layer of the primary wave, in a frame of reference defined by the perturbation. This appears to be consistent with the results of Pullin (1981) and Stern (1985), and we believed initially that our mechanism accounted for the results discussed in D1. However, further examination of evidence given by Dritschel (private communication) has shown that this may not be the case and it is now apparent that filamentation may result from several different mechanisms, and that the mechanism discussed here may be dominant in certain circumstances. This is discussed in §7.

2. Formulation

We shall consider the stability of finite amplitude progressive waves in a parallel shear flow bounded by a rigid wall. We begin by defining certain terms which will be italicized on first appearance. The fluid is assumed to be inviscid and incompressible with uniform density ρ. In Cartesian coordinates (x, y), the *basic flow* consists of irrotational flow in the x-direction with velocity $(u, v) = (0, 0)$; $0 < y < \infty$ and rotational flow with velocity $(u, v) = (-\omega y, 0)$; $-d < y < 0$, where ω is the uniform vorticity in the shear layer of mean thickness d bounded below by a rigid wall. By *disturbance* we will mean any periodic or aperiodic vorticity preserving disturbance to the *basic flow*. It is well known that the basic flow supports finite-amplitude progressive waves which we shall call *primary waves*. These have been studied by Broadbent & Moore (1985) for d finite and by Pullin & Jacobs (1986) for flow with $d \to \infty$ and with generally non-zero uniform vorticity in $y > 0$. Let λ be the wavelength of a primary wave of crest to trough height 2δ, which moves with constant speed c relative to the fluid at rest at $y \to \infty$. We shall call δ the *waveheight* of the primary wave. Then the non-uniform flow in the presence of either steady progressive, or evolutionary wave-like motion may be viewed as an irrotational and therefore a vorticity preserving *disturbance* (which may be large) on the basic flow. We denote the disturbed vorticity discontinuity (interface) by equivalent specifications

$$z_c(e, t) = x_c(e, t) + \mathrm{i} y_c(e, t), \tag{2.1a}$$

or

$$y_c = \eta(x, t), \tag{2.1b}$$

where e is an interfacial parameter, t is the time, z_c is a complex interfacial coordinate and $\mathrm{i}^2 = -1$. Using $j = 1, 2$ to denote variables in $y > \eta(x, t)$ and $y < \eta(x, t)$ respectively, the disturbance velocity (u_j, v_j) may be expressed as

$$(u_j, v_j) = \left(\frac{\partial \phi_j}{\partial x}, \frac{\partial \phi_j}{\partial y}\right) = \left(\frac{\partial \psi_j}{\partial y}, -\frac{\partial \psi_j}{\partial x}\right), \tag{2.2}$$

where ϕ_j and ψ_j are disturbance velocity potentials and stream functions respectively.

For a general unsteady disturbance to the basic flow, the boundary conditions at the interface may be written as

$$\left.\begin{aligned} \frac{\partial \eta}{\partial t}+u_1\frac{\partial \eta}{\partial x} &= v_1, \\ \frac{\partial \eta}{\partial t}+(u_2-\omega\eta)\frac{\partial \eta}{\partial x} &= v_2, \\ q_1 &= q_2. \end{aligned}\right\} \tag{2.3a, b, c}$$

Where the pressure q_j is given by

$$\frac{1}{\rho}q_1+\frac{\partial \phi_1}{\partial t}+\tfrac{1}{2}(u_1^2+v_1^2) = 0 \quad (y>\eta), \tag{2.4a}$$

$$\frac{1}{\rho}q_2+\frac{\partial \phi_2}{\partial t}+\tfrac{1}{2}(u_2^2+v_2^2)+\omega\psi_2-\omega y u_2 = 0 \quad (y<\eta). \tag{2.4b}$$

The dispersion relation for infinitesimal primary waves with wavenumber k and frequency $\sigma=\sigma_{\mathrm{R}}+\mathrm{i}\sigma_{\mathrm{I}}$ was obtained by Rayleigh (1880, 1887). Using linearized forms of (2.3)–(2.4) in which (η, ϕ_1, ϕ_2) are proportional to

$$(a_0, a_1, a_2)\exp(\mathrm{i}kx-\mathrm{i}\sigma t),$$

where

$$-\mathrm{i}\sigma a_0 = -|k|\,a_1 = ka_2\tanh(kd),$$

the dispersion relation follows as

$$\sigma a_2\{1+\operatorname{sign}(k)\tanh(kd)\} = \omega a_2\tanh(kd). \tag{2.5}$$

Thus, if $a_2 \neq 0$,

$$\sigma = \frac{\omega\operatorname{sign}(k)}{1+\coth(|k|\,d)}, \tag{2.6}$$

and $a_0, a_1 \neq 0$. For this mode it is easily shown that the total fluid velocity is continuous across the interface. There is however another solution of (2.6) with $a_1 = a_2 = 0$, $\sigma = 0$ and $a_0 \neq 0$. For this mode there is no irrotational disturbance and the total velocity is then discontinuous at the interface by an amount equal to the discontinuity in shear velocity $\omega\eta$. We shall refer to this as the 'vortex sheet' mode. It is not an allowable solution to our physical problem, since this requires continuous total velocity, but has been introduced by our use of pressure continuity (2.3*c*) rather than continuity of total velocity, for computational convenience (to allow use of existing and well-tested stability codes), as our boundary condition on $y=\eta$. Thus although (2.3*b*) is a necessary but not sufficient boundary condition, we note that for wave evolution, equality of total velocity on the interface at $t=0$, and continuity of pressure in $t>0$ ensures continuity of total velocity in $t \geqslant 0$. The vortex sheet mode will appear later as an additional and physically irrelevant solution in our stability formulation, to be recognized and discarded.

We will refer variously to dimensional and dimensionless variables, the latter based on the lengthscale λ/π and the timescale ω^{-1}. These are, respectively

$$(x,\ y,\ t,\ \lambda, \delta,\ d,\ \omega,\ c,\ u-c, v,\ \phi-cx, \psi-cy, \sigma, p\ldots),$$

$$(X, Y, T, \pi, \Delta, D, \Omega, C, U,\quad V, \Phi,\quad \Psi,\quad S, P\ldots),$$

where uppercase denotes a dimensionless variable, $\Omega=1$ is the dimensionless vorticity, p is a modulation wavenumber to be defined later and we note that the

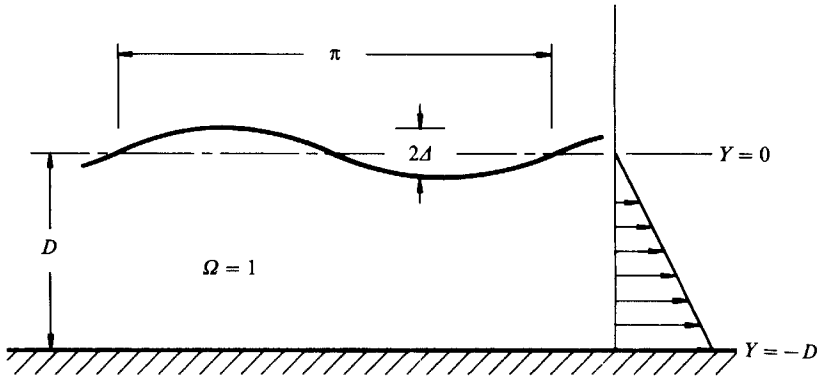

FIGURE 1. Finite amplitude wave on a uniform vortex layer of finite thickness. The flow above the wave profile is irrotational. The dimensionless wavelength is π and the amplitude is Δ.

quantities Y, V, Φ and Ψ refer to a frame of reference at rest with respect to a primary wave. We shall call $\Delta = \delta\pi/\lambda$ the *amplitude* of the primary wave. We emphasize the physical distinction between Δ and δ: the amplitude Δ is our measure of steepness and the waveheight δ is a measure of wave-extremum displacement. A primary wave on the basic flow with amplitude Δ and wavelength π is depicted in figure 1.

In §3 we utilize the nonlinear Schrödinger equation to examine modulational instability to disturbances on the basic flow when $|P| \ll 1$ and for waves of small amplitude. In §4 we briefly outline the present method of calculation for the primary wave profiles on the vortex layer. Section 5 describes the spectral calculations for the stability of the primary wave states of §4 to general subharmonic perturbations with wavenumber p. In the limit of small Δ, the instabilities found correspond to the well-known quartet wave resonance (e.g. McLean 1982) with growth rate scaling on Δ^2. Over the range of Δ studied, $0.005\pi \leqslant \Delta \leqslant 0.5\pi$, we find instability for $D/\pi = d/\lambda$ in the range $0.094 < D/\pi < 1.7$ and stability otherwise. In §6 we describe initial-value calculations using the CD method with an initial disturbance consisting of a primary wave plus an eigenvector provided by the spectral calculation. We shall refer to the eigenvector as an infinitesimal *perturbation* to the primary wave. For several specific cases we find waveheight growth and vorticity interface filamentation when $P = 1$ (first subharmonic instability) and $D/\pi = 0.4$, $D/\pi = 0.5$, but stable propagation of the disturbance for the spectrally stable flow with $D/\pi = 2.0$ over the finite period of numerical simulation. The implications of the present results for the filamentation phenomenon are discussed, and a plausible mechanism is put forward based on examination of velocity vector plots for a particular realization.

3. Nonlinear Schrödinger equation

The nonlinear Schrödinger equation (NLS) describes the evolution of long-wavelength perturbations to waves of small amplitudes. For plane two-dimensional flow the relevant equation is (Pullin & Grimshaw 1986)

$$\mathrm{i}\frac{\partial \eta_1}{\partial \tau} + \hat{\lambda}\frac{\partial^2 \eta_1}{\partial \xi^2} + \nu|\eta_1|^2\eta_1 = 0, \tag{3.1}$$

where $\tau = \hat{\epsilon}^2 t$, $\xi = \hat{\epsilon}(x - Vt)$ are scaled time and length variables respectively, $\hat{\epsilon}\eta_1$ is the complex wave amplitude $V = \partial\sigma/\partial k$ is the group velocity, $\hat{\lambda} = \frac{1}{2}\partial V/\partial k$, $\hat{\epsilon}$ is a small

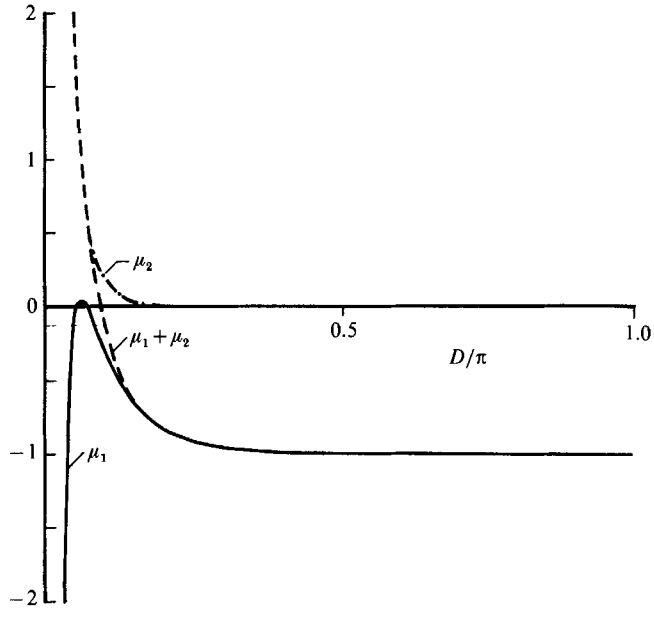

FIGURE 2. Variation of terms contributing to ν in (3.5b), where $\mu_1 = -\frac{1}{2}(\hat{S}-3)(\hat{S}^2-2\hat{S}-1)/(\hat{S}+1)$, $\mu_2 = (\hat{S}-1)^2/(2kd(\hat{S}+1))$. $\hat{S} = \coth(kd)$.

parameter and the coefficient ν is determined by the interaction of the second harmonic and the wave induced mean flow with the basic wave. To leading order the basic wave is $\eta = 2\mathrm{Re}\{\hat{\epsilon}\eta_1 \exp(\mathrm{i}k_0 x - \mathrm{i}\sigma_0 t)\}$ where $\sigma_0 = \sigma_0(k_0)$ is given by (2.6) and $k_0 = 2\pi/\lambda_0$ is the wavenumber of the basic wave. Both V and λ are to be evaluated at $k = k_0$. The plane wave solution to (3.1a) may be written as

$$\eta_1 = A \exp(\mathrm{i}\nu|A|^2\tau), \tag{3.2}$$

where $\hat{\epsilon}|A| = \frac{1}{2}\delta$. The modulational perturbations are long waves with amplitude proportional to $\mathrm{Re}\{\exp(\mathrm{i}\hat{p}\xi - \mathrm{i}\hat{\sigma}\tau)\}$ where $\hat{\sigma} = \hat{\epsilon}^{-2}\sigma$ and $\hat{p} = \hat{\epsilon}^{-1}p$ are the scaled frequency and modulation wavenumbers respectively. There is instability when $0 < \hat{p}^2 < 2\nu\hat{\lambda}^{-1}|A|^2$. This requires $\hat{\lambda}\nu > 0$, and the growth rate $\hat{\sigma}_\mathrm{I}(\hat{\sigma} = \hat{\sigma}_\mathrm{R} + \mathrm{i}\hat{\sigma}_\mathrm{I})$ is then given by

$$\hat{\sigma}_\mathrm{I}^2 = \hat{\lambda}\hat{p}^2(2\nu|A|^2 - \hat{\lambda}\hat{p}^2). \tag{3.3}$$

The maximum growth rate and corresponding wavenumber are respectively

$$\max_{\hat{p}}(\hat{\sigma}_\mathrm{I}) = |\nu|\,|A|^2, \tag{3.4a}$$

$$p_{\max} = (\hat{\lambda}^{-1}\nu)^{\frac{1}{2}}|A|, \tag{3.4b}$$

while the bandwidth is $\Delta\hat{p} = \sqrt{2}\hat{p}_{\max}$.

The quantities V and $\hat{\lambda}$ follow from (2.6) and the coefficient ν may be obtained from the analysis of Pullin & Grimshaw (1986) for the modulational instability of shear-gravity flows in a two-layer fluid. Omitting the algebra, the results are

$$V = \omega d\,\mathrm{e}^{-2kd}, \quad \hat{\lambda} = -\omega d^2\,\mathrm{e}^{-2kd}, \tag{3.5a}$$

$$\nu = \tfrac{1}{2}\omega k^2\left\{-\frac{(\hat{S}-3)(\hat{S}^2-2\hat{S}-1)}{(\hat{S}+1)} + \frac{1}{kd}\frac{(\hat{S}-1)^2}{(\hat{S}+1)}\right\}, \tag{3.5b}$$

where $\hat{S} = \coth(kd)$. In (3.5*b*) the terms in curly brackets represent respectively the contribution to ν arising from the interaction of the basic wave with the second harmonic and with the wave-induced mean flow. Their variation with $D/\pi = d/\lambda$ is shown in figure 2. From (3.5*a*) it follows that $\hat{\lambda} < 0$ always, so instability thus requires $\nu < 0$. This agrees with Benney & Maslowe (1975) as corrected by Balagondar, Maslowe & Melkonian (1987).

The limit $kd = 2\pi d/\lambda \to \infty$, i.e. infinite depth of the shear layer, requires some comment. Here, the linear solution oscillates at fixed frequency $\sigma = -\frac{1}{2}\omega$ for all k. Hence by Fourier superposition there exists a solution $\eta = \exp(\mathrm{i}\omega t) f(x)$ where $f(x)$ is arbitrary. The group velocity V becomes zero in this limit but there exists nonlinear dispersion. Furthermore $\hat{S} \to 1$ and from (3.5*a*, *b*) $\nu \to -\omega k^2$ and $\lambda \to 0$ but remains negative. Hence the NLS predicts instability with $\max_p(\hat{\sigma}_\mathrm{I})$ asymptotic to $|\omega||kA|^2$, at wavenumber

$$(p_{\max} d)^2 = (kd)^2 \mathrm{e}^{2kd} |A/d|^2. \tag{3.6}$$

This result is not consistent with the scaling for the nonlinear Schrödinger equation which requires p small. The limit $kd \to \infty$ is therefore outside the range of validity of the NLS.

4. Finite amplitude waves on a vortex layer

In §5 and §6 we shall study respectively the linear stability and the nonlinear evolution of primary waves subject to a general subharmonic perturbation, but it is first necessary to calculate the interface profiles corresponding to the primary waves. The numerical method is essentially that used by Pullin & Jacobs (1986), so only brief details are given here. In the frame of reference moving with the wave speed C (we employ dimensionless coordinates), the boundary conditions defining the wave shape may be expressed in the form of an integro-differential equation for $Z_\mathrm{c}(e) = X_\mathrm{c}(e) + \mathrm{i}Y_\mathrm{c}(e)$, namely

$$\mathrm{Im}\left\{(U_\mathrm{t} - \mathrm{i}V_\mathrm{t})_{\mathscr{I}} \frac{\mathrm{d}Z_\mathrm{c}}{\mathrm{d}e}\right\} = 0, \tag{4.1}$$

where $\mathscr{I}$ denotes the interface, and $U_\mathrm{t} - \mathrm{i}V_\mathrm{t}$ is the total dimensionless complex velocity given by, on $\mathscr{I}$

$$U_\mathrm{t} - \mathrm{i}V_\mathrm{t} = -\frac{\Omega}{2\pi\mathrm{i}} \int_0^\pi \left\{(Y_\mathrm{c} - Y_\mathrm{c}') \cot(Z_\mathrm{c} - Z_\mathrm{c}') \frac{\mathrm{d}Z_\mathrm{c}'}{\mathrm{d}e'} + (Y_\mathrm{c} + Y_\mathrm{c}') \cot(Z_\mathrm{c} - Z_\mathrm{c}^{*\prime} + 2\mathrm{i}D) \frac{\mathrm{d}Z_\mathrm{c}^{*\prime}}{\mathrm{d}e'}\right\} \mathrm{d}e' - \Omega Y_\mathrm{c} - C. \tag{4.2}$$

In (4.2), $Z_\mathrm{c} = Z_\mathrm{c}(e)$, $Z_\mathrm{c}' = Z_\mathrm{c}(e')$ and $\Omega = 1$. An additional condition is required to define the wave uniquely by specifying the amplitude A as

$$(Y_\mathrm{c})_{\max} - (Y_\mathrm{c})_{\min} = 2A. \tag{4.3}$$

Numerical solutions are found in a standard way by expanding $Z_\mathrm{c}(e)$ as a truncated Fourier series

$$Z_\mathrm{c}(e) = e + A_1 \sin(2e) + \mathrm{i} \sum_{n=0}^{N-1} B_n \cos(2ne). \tag{4.4}$$

We thus consider only waves symmetrical about crest or trough. The quantity A_1 is fixed in order to concentrate points near either the wave crest or trough and we determine the B_n, $n = 0, \ldots, N-1$ and C by satisfying (4.1)–(4.2) at $e_j = j\pi/(2N)$, $j = 1, \ldots, N-1$. The two closure equations are (4.3) and the requirement that the mean

wave level be $Y = 0$. Calculations were performed with $N = 40$ in 14-figure arithmetic. Only waves of moderate amplitude compared to the limiting wave were calculated with $\Delta = 0.005\pi$, 0.01π, 0.025π and 0.05π. This is because convergence difficulties were encountered in the subharmonic spectral calculations for waves with larger Δ (see §5). The values of D considered were $D/\pi = d/\lambda = 0.02$–0.10 (0.02), 0.15, 0.2–0.8 (0.1), 1.0, 1.25, 1.5, 1.7, 2.0, 2.5, 5 and ∞. Calculations at $D/\pi = 0.9$ were also done with $\Delta = 0.05\pi$.

5. Spectral calculations of subharmonic instability

From (3.5*b*), the NLS predicts modulational instability of primary waves on a wall-bounded uniform vortex layer of mean thickness d when $d/\lambda > 0.094$. When Δ is small the mechanism of the instability may be interpreted as the well-known quartet-resonant interaction operating between two components of the main wave with wavenumber k_0, and two sideband components, with wavenumbers chosen as $p-k_0$ and $p+k_0$ respectively, so as to satisfy the appropriate resonance condition. Pullin & Jacobs (1986) performed spectral calculations of general subharmonic instability in the limit $D/\pi \to \infty$ and found stability for all p. In order to examine the wave stability properties when d is finite we calculated numerically the stability of the primary wave states described in §4. The numerical method is an application of that described by Pullin & Grimshaw (1986), which in turn was derived from the technique developed by McLean (1982) (see also McLean *et al.* 1981) for the calculation of water-wave instability. Since the present implementation differs from that of Pullin & Grimshaw only in that gravity is absent and the fluid density is uniform, we give only a brief outline.

We use dimensionless variables as described in §2 and choose a frame of reference at rest with respect to the steady non-uniform flow given by the primary waves of §4. We consider disturbances to the basic flow given by

$$Y_c = \bar{Y}_c(X) + \epsilon Y'_c(X, T), \tag{5.1a}$$

$$\Phi_j = \bar{\Phi}_j(X, Y) + \epsilon \phi'_j(X, Y, T) \quad (j = 1, 2), \tag{5.1b}$$

$$\Psi_2 = \bar{\Psi}_2(X, Y) + \epsilon \psi'_2(X, Y, T), \tag{5.1c}$$

where barred quantities are solutions for the primary waves, Y'_c, ϕ'_j and ψ'_2 are perturbations, $\epsilon \ll 1$ is the perturbation amplitude and the perturbation waveheight ($\frac{1}{2}$ crest to trough) is $O(\epsilon\lambda/\pi)$. Next we substitute (5.1) into (2.2)–(2.4), expand in powers of ϵ about the primary wave solution and retain terms of $O(\epsilon)$. This gives a set of boundary conditions to be satisfied on $Y = \bar{Y}_c(X)$ which are linear in Y'_c, ϕ'_j and ψ'_2. We note that this procedure differs from that of Pullin & Jacobs who used boundary conditions consisting of the wave kinematic condition together with specification of equal total-fluid velocity on either side of the interface. We now seek solutions, which automatically satisfy $\nabla^2\phi'_1 = \nabla^2\phi'_2 = \nabla^2\psi'_2 = 0$, of the form

$$Y'_c = \exp(-\mathrm{i}ST + \mathrm{i}PX) \sum_{-\infty}^{\infty} a_m \exp(2\mathrm{i}mX), \tag{5.2a}$$

$$\phi'_1 = \exp(-\mathrm{i}ST + \mathrm{i}PX) \sum_{-\infty}^{\infty} b_m \exp(2\mathrm{i}mX) \exp(-R_m Y), \tag{5.2b}$$

$$\psi_2' = \exp(-\mathrm{i}ST + \mathrm{i}PX) \sum_{-\infty}^{\infty} \hat{c}_m \exp(2\mathrm{i}mX) \frac{\sinh[R_m(Y+D)]}{\cosh[R_m D]}, \tag{5.2c}$$

$$\phi_2' = \exp(-\mathrm{i}ST + \mathrm{i}PX) \sum_{-\infty}^{\infty} c_m \exp(2\mathrm{i}mX) \frac{\cosh[R_m(Y+D)]}{\cosh[R_m D]}, \tag{5.2d}$$

where $R_m = |2m+P|$, $\hat{c}_m = c_m \operatorname{sign}(2m+P)$, $S = S_R + \mathrm{i}S_I$ is the dimensionless complex frequency and P; $0 < P < 2$ is the modulation wavenumber. Use of (5.2) in the linearized boundary conditions gives an eigenvalue problem with eigenvector $[a_m, b_m, c_m]^T$, $m = -\infty, \ldots, \infty$ and eigenvalue S. The assumed symmetry properties of the basic wave may be used to show that eigenvalues are either purely real or occur in conjugate pairs. Hence spectral instability corresponds to finding an eigenvalue with $S_I \neq 0$.

The calculations were performed by first truncating the series in (5.2) at $m = M$ terms. The linearized boundary conditions were then applied at $2M+1$ equally spaced points on the primary wave profile $Y_c = \bar{Y}_c(X; D, \Delta)$ in $0 \leqslant X \leqslant \pi$. This gives a $(6M+3) \times (6M+3)$ discrete eigenvalue problem which was solved numerically by standard methods based on the QZ algorithm. Of the $6M+3$ eigenvalues produced in each specific calculation, $2M+1$ correspond to linear modes propagating on the non-uniform flow given by the steady primary wave, with continuous total velocity across the perturbed vorticity jump. These are solutions for our physical problem and it is within these modes that instabilities, if they exist, must appear. A further $2M+1$ eigenvalues correspond to finite-amplitude realizations of the vortex-sheet mode discussed in §2, and finally there is a $(2M+1)$-fold degenerate infinite eigenvalue which appears owing to the linear interdependence of the coefficients in (5.2): there are only $4M+2$ linearly independent modes. The $2M+1$ vortex-sheet modes are spurious insofar as our physical problem is concerned and must be discarded. They are easy to recognize since there is no associated velocity field perturbation, i.e. $b_m = c_m = 0$, $a_m = 0$, $m = -M, \ldots, M$, in (5.2). Moreover, quite general arguments based on evolution equations for the tangential velocity jump across the interface in infinitesimal perturbations to the steady flow of the primary wave may be used to show that there can be no modulational-type instability associated with the vortex-sheet mode. Hence any unstable eigenvalues produced in the spectral calculations represent modulational instability of finite amplitude primary waves on the vortex layer.

When $\Delta \to 0$, the physically relevant dimensionless eigenvalues are given by, from (2.6)

$$S_m = -C_0(P+2m) + \operatorname{sign}(P+2m)[1+\coth(D|P+2m|)]^{-1}, \tag{5.3}$$

where $C_0 = \frac{1}{2}[1+\coth(2D)]^{-1}$ is the linearized dimensionless phase speed of the primary wave, corresponding in (5.3) to $P = 0$, $m = 1$, $S_1 = 0$. In this limit and when $P \ll 1$, the modulational instability described by the NLS of §3 should apply. When $\Delta > 0$ and P is not small, the appearance of instability is expected to be associated with the coalescence of distinct eigenvalues, say $S_{m_1}(P; \Delta, D)$ and $S_{m_2}(P; \Delta, D)$ into a conjugate pair, and in the limit of small Δ, the quartet resonance corresponds to $m_{1,2} = \pm 1$. Further, it may be shown that $S_m(P; \Delta, D) = -S^*_{-(m+1)}(2-P; \Delta, D)$, and we note that this is satisfied by (5.3). Using this and similar results for the eigenvectors in each of (5.2), it follows that any solution of the eigenvalue problem with wavenumber P has a physically equivalent solution corresponding to wavenumber $2-P$. This is sufficient to show that there are always two solution branches when $0 < P < 2$, which together give symmetry about $P = 1$. Hence it is

always sufficient to perform calculations with $0 < P \leqslant 1$ and to infer results for $1 < P < 2$ from symmetry and the second branch. For display purposes it is convenient to show results for a single branch in $0 < P < 2$.

Calculations were performed for the values of D specified in §4. For each D, primary waves of amplitude $\Delta = 0.005\pi$, 0.001π, 0.025π and 0.05π respectively were tested for instability at values of $P = 0.01$–0.10 (0.01), 0.12–0.90 (0.02) and 0.91–1.00 (0.01). Where instabilities with narrow bandwidth were detected, smaller increments in P were used locally. Results were obtained with $M = 10$–30 coefficients in the eigenfunction expansion for the perturbation (5.2), with $\Delta = 0.005\pi$, 0.001π and 0.025π, but it was found that $M = 40$ was required for satisfactory convergence of the eigenvalues as M was increased for $\Delta = 0.05\pi$. Some calculations at $\Delta = 0.075\pi$ were attempted but these were not successful with $M = 40$, which was the largest value we could use within the limits of our available computing resource.

The present numerical stability results with $\Delta > 0$ are depicted in figures 3–6, where curves of S_{I}/Δ^2 versus P are shown with Δ and D fixed. The scaling S_{I}/Δ^2 is suggested by the NLS predictions and also by the well-known generic result for an $(N+2)$th-order wave resonance where growth rates are expected to be $O(\Delta^N)$. The qualitative trends shown in figures 3–6 are similar for each of the four values of Δ treated here. These trends are conveniently discussed in terms of the (dimensional) quantities

$$\sigma_{\max} = \max_{p} [\sigma_{\mathrm{I}}(p; \delta, d)], \tag{5.4}$$

the maximum growth rate at fixed δ and d, $p_{\max}$, the value of p corresponding to $\sigma_{\max}$, and Δp, the bandwidth of the instability. Dimensional analysis gives

$$\sigma_{\max} = \frac{\delta^2 \omega \pi^2}{\lambda^2} f_1\left(\frac{d}{\lambda}, \frac{\delta}{\lambda}\right), \tag{5.5a}$$

$$p_{\max} = \frac{\pi^2 \delta}{\lambda^2} f_2\left(\frac{d}{\lambda}, \frac{\delta}{\lambda}\right), \tag{5.5b}$$

$$\Delta p = \frac{\pi^2 \delta}{\lambda^2} f_3\left(\frac{d}{\lambda}, \frac{\delta}{\lambda}\right). \tag{5.5c}$$

Denoting the dimensionless forms of $(\sigma_{\max}, p_{\max}, \Delta p)$ by $(S_{\max}, P_{\max}, \Delta P)$ respectively, based on the lengthscale λ/π and the timescale ω^{-1}, it follows that $f_1 \equiv S_{\max}\Delta^{-2}$, $f_2 \equiv P_{\max}\Delta^{-1}$ and $f_3 \equiv \Delta P \Delta^{-1}$. Plots of $\sigma_{\max}$ and ΔP versus $d/\lambda = D/\pi$ at fixed $\Delta/\pi = \delta/\lambda$, obtained from the eigenvalue calculations, are shown in figures 7–8. Also shown are predictions of the NLS obtained from (3.3)–(3.6). Note that the measure of scaled primary wave amplitude appropriate to the NLS calculations of §3 and the present amplitude Δ are related as $\Delta = 2\pi\hat{\epsilon}|A|/\lambda$ (or $\delta = 2\hat{\epsilon}|A|$: ϵ and $\hat{\epsilon}$ have different meaning). Equations (3.4)–(3.5) predict that f_1, f_2 and f_3 of (5.5) depend only on D/π, and hence the NLS predictions appear as single (solid) lines in figures 7–8. There is good agreement between the results given by the NLS and the spectral calculations at small D/π in figures 7–8; both predict stability at $D/\pi < 0.094$. At larger D/π the spectral calculations show dependence of f_1–f_3 on Δ/π. As D/π increases further, figures 3–6 indicate detachment of the instability bands from $P = 0$ and a subsequent reduction in both ΔP and $S_{\max}$ for each of the four values of Δ examined. No instability could be detected at our values of Δ with $D/\pi = 1.70$, 2.0, 2.5, 5.0 and ∞ respectively. When $\Delta/\pi = 0.005$, which shows the largest bandwidth at $D/\pi = 1.50$,

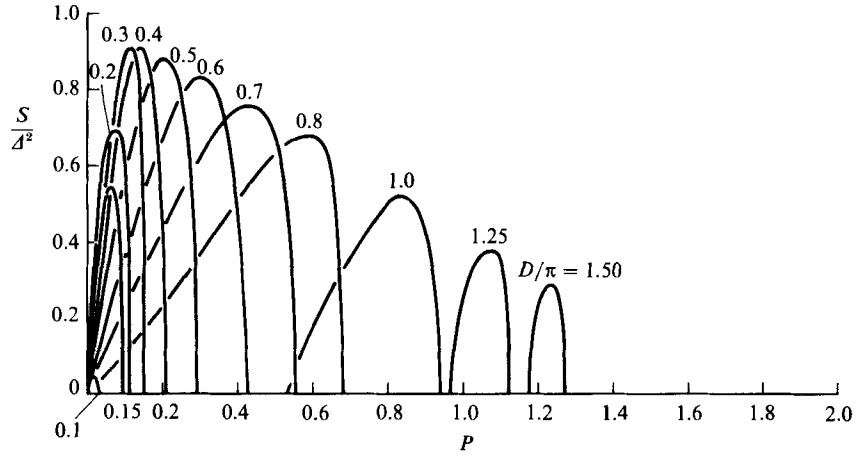

FIGURE 3. Calculated growth rate of finite amplitude instability, $\Delta/\pi = 0.005$. Values of D/π as shown.

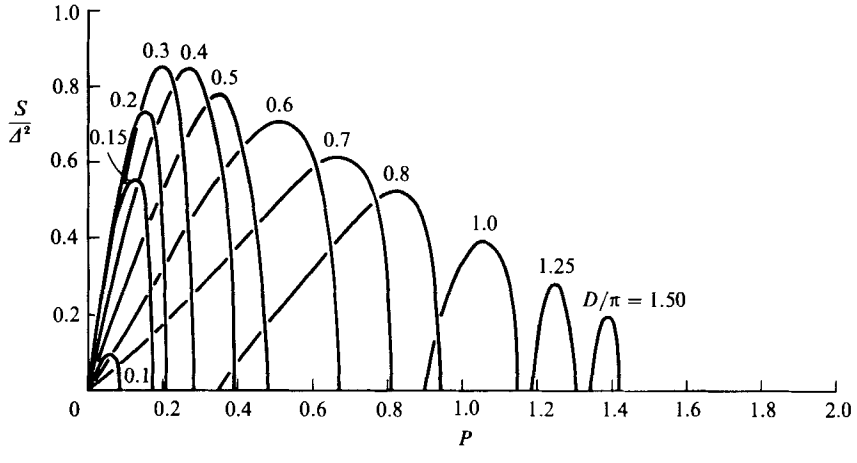

FIGURE 4. For legend, see figure 3. $\Delta/\pi = 0.01$, values of D/π as shown.

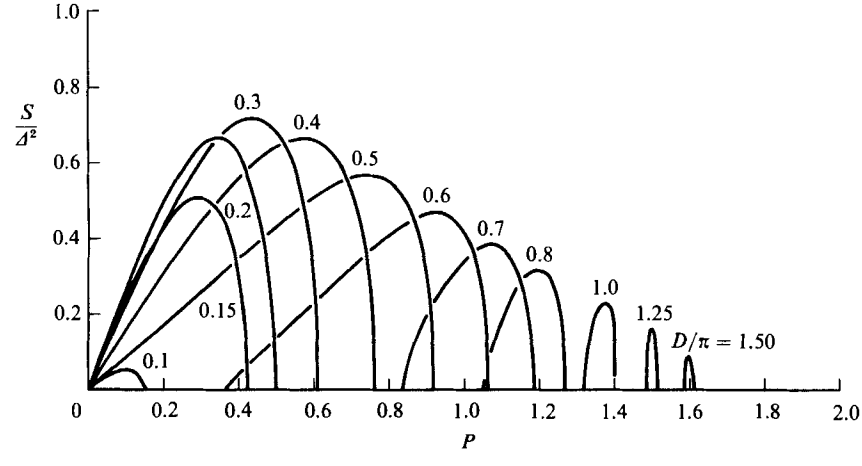

FIGURE 5. For legend, see figure 3. $\Delta/\pi = 0.025$, values of D/π as shown.

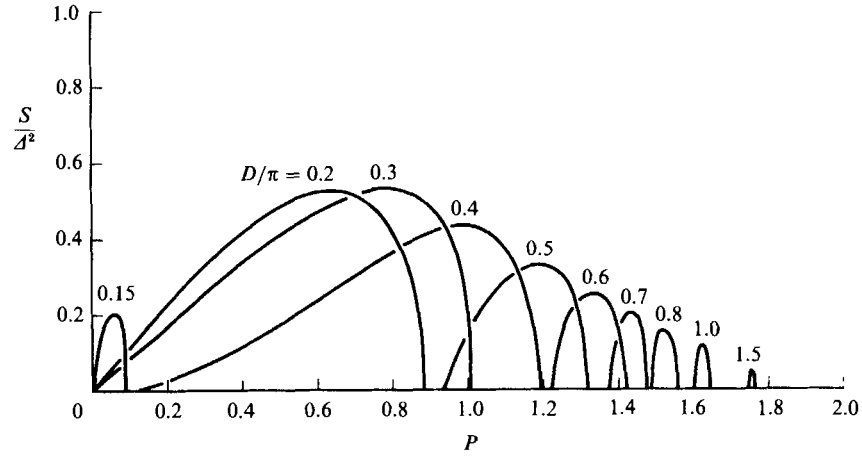

FIGURE 6. For legend, see figure 3. $\Delta/\pi = 0.050$, values of D/π as shown.

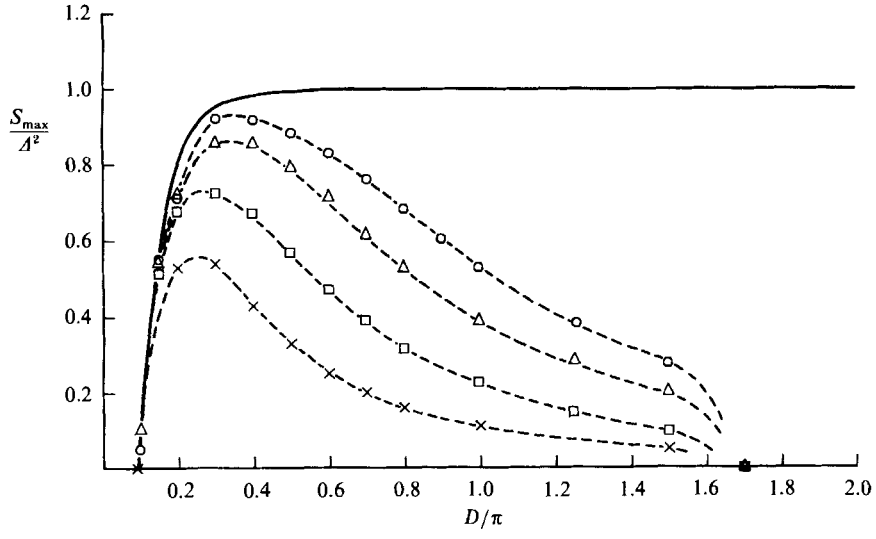

FIGURE 7. Maximum growth rate of instability 0, $\Delta/\pi = 0.005$; △, $\Delta/\pi = 0.01$; □, $\Delta/\pi = 0.025$; ×, $\Delta/\pi = 0.05$; ——, nonlinear Schrödinger equation.

the search was conducted at $P = 1.35$–$1.65\,(0.005)$ for $D/\pi = 1.70$. Hence any instability band in this range of P must have $\Delta P < 0.005$.

From the spectral results we conclude that the finite amplitude progressive primary waves of wavelength π on a uniform vortex layer of mean thickness D are unstable to general subharmonic disturbances when

$$0.094 < D/\pi < 1.7. \tag{5.6}$$

This result appears to hold independent of Δ over the range of Δ tested. It is thus the lengthscale ratio D/π that controls the instability and the main effect of Δ is that the growth rate of the instability scales approximately on Δ^2. The result is also consistent with the related calculations of Pullin & Jacobs (1986) who, using a different implementation of the boundary conditions to that employed here found stability when $D \to \infty$.

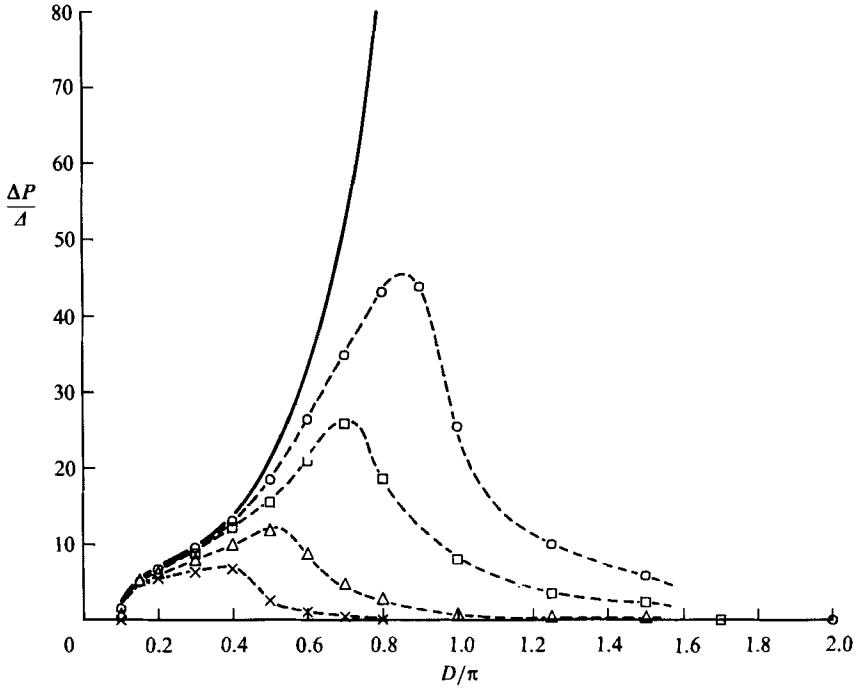

FIGURE 8. Bandwidth of instability. For key, see figure 7.

6. CD simulation of nonlinear wave evolution

The results of §5 suggest a mechanism whereby finite amplitude primary waves of arbitrarily small A and with wavelengths in the range given by (5.6) may grow in waveheight by an instability which at $\delta \ll \lambda$ is a resonant interaction. In order to examine the possible relevance of this instability to the interfacial filamentation phenomenon discussed in §1, we performed contour dynamical (CD; see Deem & Zabusky 1978*a*) calculations of the nonlinear wave evolution using as initial conditions a disturbance to the basic flow comprising a primary wave with a superposed perturbation consisting of an eigenvector provided by the spectral calculations. We utilize dimensionless coordinates and consider a computational domain consisting of n wavelengths in the X-direction of the primary wave where n is a positive integer. The CD implementation is that of Jacobs & Pullin (1985) to which we refer the reader for numerical details. The full evolutionary equations are

$$\frac{\partial Z_c^*}{\partial T} = -\frac{\Omega}{2\pi i}\int_{\mathscr{S}}\left\{(Y_c - Y_c')\cot\left[\frac{1}{n}(Z_c - Z_c')\right]\frac{dZ_c'}{de'} + (Y_c + Y_c')\cot\left[\frac{1}{n}(Z_c - Z_c'^* + 2iD)\right]\frac{dZ_c'^*}{de'}\right\}de' - \Omega Y_c, \quad (6.1)$$

where $Z_c^*(e, T)$, $0 < e < n\pi$ is the Lagrangian description of the interface shape, and we note that (6.1) describes the wave evolution in a frame of reference at rest with respect to the fluid at $Y \to \infty$.

We choose initial conditions in the form of (5.1*a*) and (5.2*a*) with Y_c' in (5.2*a*) evaluated at $T = 0$. The coefficients a_m, $m = -M, \ldots, M$ provided by the spectral

calculations are normalized such that $\max[Y_c'(X,0)] - \min[Y_c'(X,0)] = 2$, and the coefficient of maximum amplitude is purely real. Hence from (5.1*a*) and (5.2*a*) ϵ is the dimensionless amplitude of the perturbation (waveheight $= \epsilon\lambda/\pi$), corresponding to subharmonic wavenumber P.

The CD calculations were done using four primary wave states with properties summarized in table 1. Of these one wave is spectrally stable while the other three exhibit instability and were chosen to span a moderate range of Δ, $0.035 < \Delta/\pi < 0.05$. We would have liked to perform calculations with the smaller amplitude $\Delta/\pi = 0.025$ but tests with $D/\pi = 0.6$ proved indecisive as the growth rate of the waveheight was too small. The value of P was chosen as $P = 1.0$ for all cases. Hence the disturbance wavelength is 2π (first subharmonic) and $n = 2$ in (6.1). With $D/\pi = 0.4$ and $D/\pi = 0.5$ this choice exhibits subharmonic instability at near the maximum growth rate, while with $D/\pi = 2.0$, the spectral calculations indicate absolute stability to perturbations of infinitesimal amplitude. Typical spectra calculated as in §5 for two of the primary wave states, one stable and one unstable, are shown in tables 2–3 where we tabulate the first seven eigenvalues with $S_R < 0$.

We report the results of seven CD simulations of wave evolution with initial conditions as described previously. The results of four simulations are shown graphically in figures 9–12, where each figure shows a sequence of wave profile shapes with increasing T as indicated. For most simulations the initial number of points on the interface was $N = 400$ and these were spaced equally in X. In cases where filamentation occurred, N increased rapidly. Simulations were terminated when either N reached $N_{max} = 1500$ or when the fractional change in area in $0 \leqslant X \leqslant 2\pi$, $-D \leqslant Y \leqslant Y_c(e,t)$ exceeded 10^{-4}. No 'contour surgery' style algorithm was employed: our main aim was to examine the onset of filamentation rather than its long-timescale state.

In figure 9 the parameters are $D/\pi = 0.4$, $\Delta/\pi = 0.05$, $\epsilon = 0$ corresponding to the unperturbed primary wave. The CD calculations showed wave propagation with unchanging form over some $20T_w$, where T_w is the wave period. Figure 10 shows a simulation with $D/\pi = 2.0$, $\Delta/\pi = 0.05$. The perturbation was chosen as a stable eigenvector with amplitude $\epsilon/\pi = 0.005$. This and a similar calculation (not shown) with the same D, Δ and ϵ but with a different initial perturbation eigenvector both showed no tendency towards filament formation over some $20T_w$. Close examination of the interface crest and trough displacements showed that these did not tend to grow with time but appeared to oscillate about the equilibrium value with amplitude roughly equal to ϵ as would be expected from linear theory.

Figure 11 shows the case $D/\pi = 0.40$, $\Delta/\pi = 0.05$, $\epsilon/\pi = 0.005$ with the perturbation now chosen as the unstable eigenvector with growth rate shown in table 2. In this case it was found that the Y-displacement of both profile troughs showed oscillation accompanied by slow growth. At $T = 94.08$ in figure 11 the slope becomes large and the interface overturns near $T = 95.28$, leading to subsequent intrusive filamentation, that is the filament grows into the vortical layer. The filamentation repeats after approximately T_w in agreement with the results of D1 although as will be discussed subsequently we believe the mechanism to be different. In figure 12 again $D/\pi = 0.40$, $\Delta/\pi = 0.05$, $\epsilon/\pi = 0.005$ but in this case the disturbance contains a perturbation which is not an unstable eigenvector. Again there is filamentation but it is delayed compared to the case of figure 11. In table 4 we summarize the results of three simulations where the disturbance consists of the primary wave plus the unstable eigenvector. For each case there is filamentation at time tabulated as

$D\pi$	Δ/π	C	T_w	$\bar{Y}_{min}$	S_I
2.0	0.05	0.262281	11.9780	—	0
0.4	0.05	0.260474	12.0611	−0.183584	0.01069
0.5	0.04	0.257386	12.2058	−0.142170	0.00654
0.5	0.035	0.255550	12.2935	−0.122458	0.00530

TABLE 1. Primary wave states used in Contour Dynamical calculations. C is the primary wave speed, T_w the period, $\bar{Y}_{min}$ the displacement of the wave trough and S_I is the maximum growth rate of the subharmonic instability with $P = 1$

$S_R(\Delta = 0)$	m	S_R	S_I	m'
-0.21114×10^0	−1	-0.20715×10^0	0.10692×10^{-1}	1
-0.25434×10^0	1	-0.20715×10^0	0.10692×10^{-1}	1
-0.74180×10^0	2	-0.67247×10^0	0	2
-0.12385×10^1	3	-0.11415×10^1	0	3
-0.17352×10^1	4	-0.16105×10^1	0	4
-0.22320×10^1	5	-0.20797×10^1	0	5
-0.27287×10^1	6	-0.25492×10^1	0	6

TABLE 2. Portion of calculated spectrum $D/\pi = 0.40$, $\Delta/\pi = 0.05$, $P = 1$. m labels the eigenvalue for $\Delta = 0$ (equation (5.3)). m' labels $a_{m'}$ with the maximum magnitude in the eigenvector. Only eigenvalues with $S_R < 0$ are shown since for $P = 1$, the spectrum is antisymmetric about $S = 0$.

$S_R(\delta = 0)$	m	S_R	S_I	m'
-0.25000×10^0	−1	-0.21213×10^0	0	1
-0.25000×10^0	1	-0.24652×10^0	0	−1
-0.75000×10^0	2	-0.68061×10^0	0	1
-0.12500×10^1	3	-0.11529×10^1	0	3
-0.17500×10^1	4	-0.16252×10^1	0	5
-0.22500×10^1	5	-0.20976×10^1	0	4
-0.27500×10^1	6	-0.25703×10^1	0	5

TABLE 3. For legend, see table 2. $D/\pi = 2.0$, $\Delta/\pi = 0.05$, $P = 1$

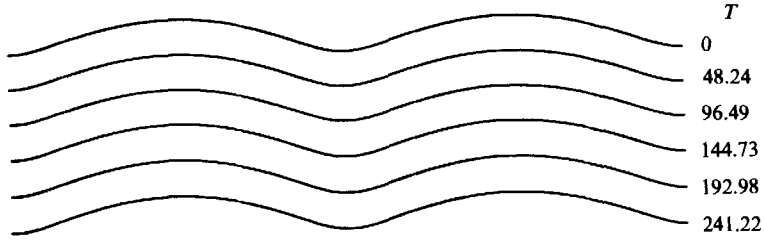

FIGURE 9. Evolution of vorticity interface (wave profile) calculated using contour dynamics. Each wave profile is depicted in a frame of reference in which flow at $Y \to \infty$ is stationary. Dimensionless times T as shown. The computational domain in the X-direction is of length $2 \times$ basic wavelength $= 2\pi$. The flow above the interface is irrotational and the flow below has unit vorticity. Parameters: $D/\pi = 0.40$, $\Delta/\pi = 0.05$, $\epsilon = 0$ (no perturbation). Primary wave speed $C = 0.260474$ and period $T_w = 12.0611$.

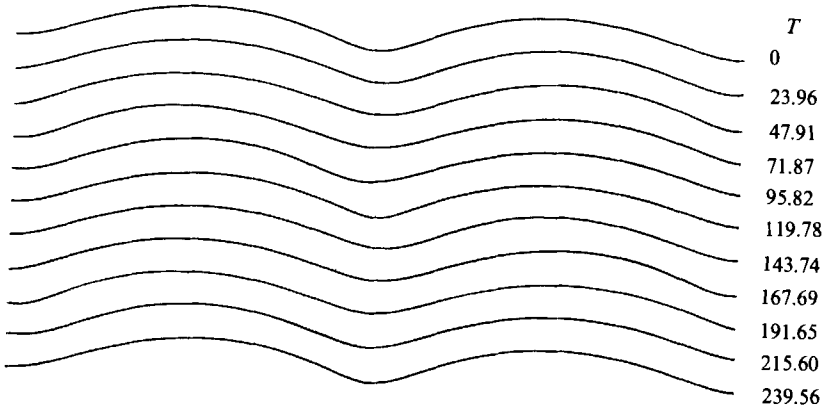

FIGURE 10. For legend, see figure 9. Basic wave $D/\pi = 2.0$, $\Delta/\pi = 0.05$. Perturbation is stable eigenvector with $P = 1$, $\epsilon/\pi = 0.005$.

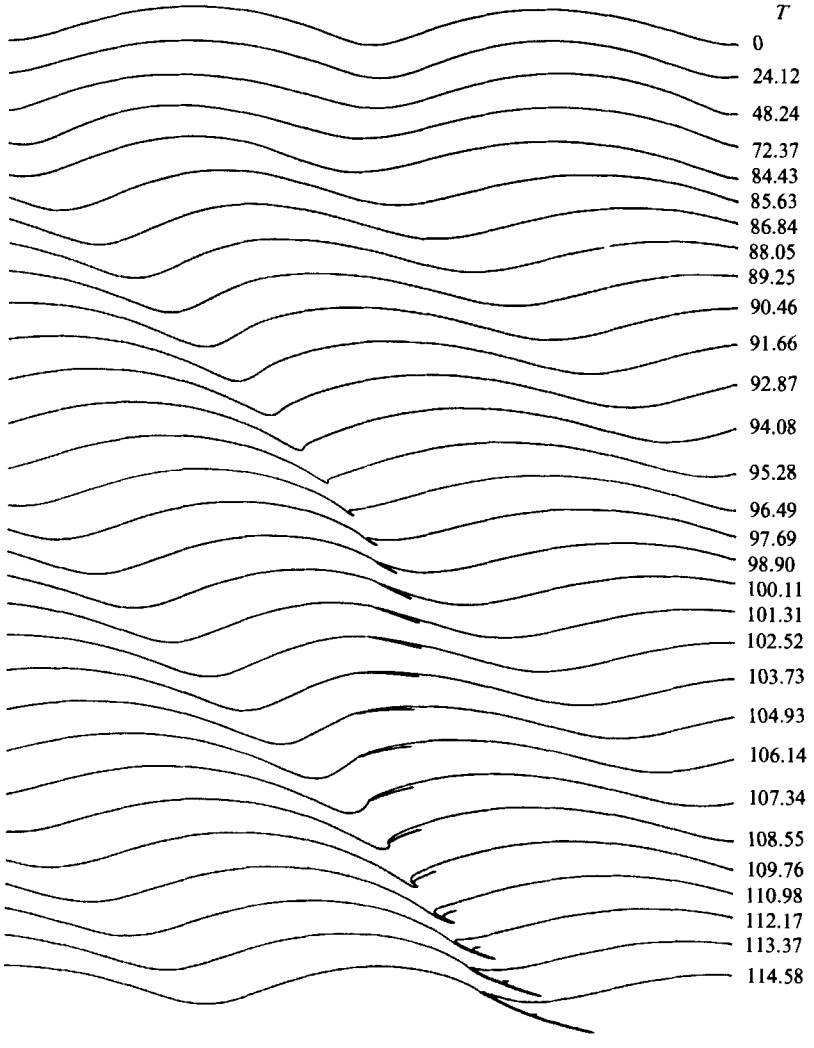

FIGURE 11. For legend, see figure 9. Basic wave $D/\pi = 0.40$, $\Delta/\pi = 0.05$. Perturbation is unstable eigenvector (see table 2). $P = 1$, $\epsilon/\pi = 0.005$.

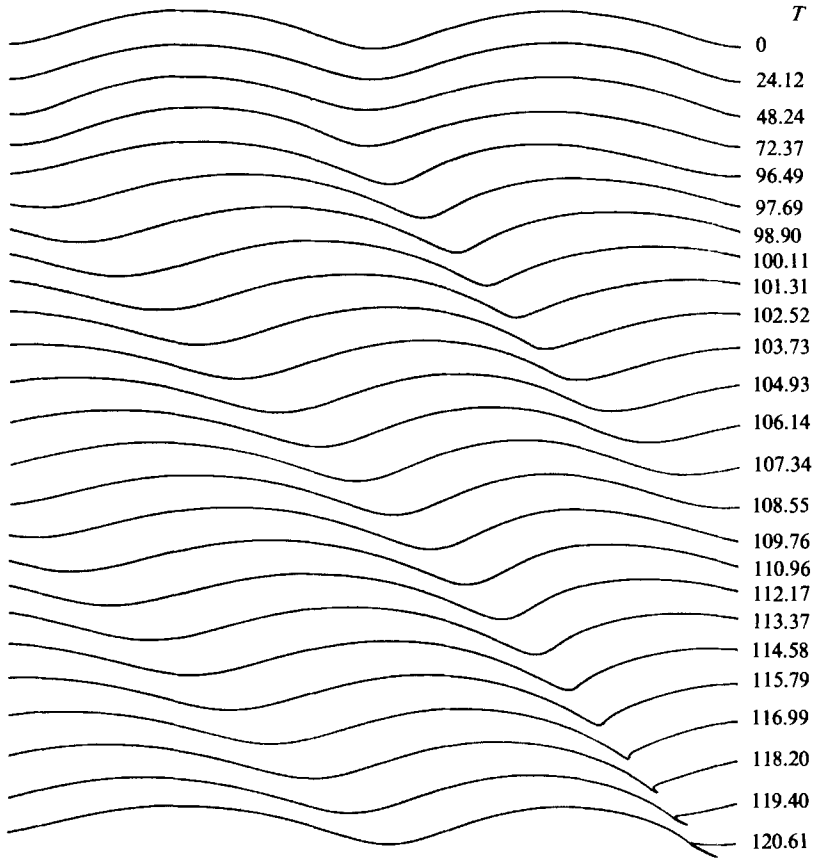

FIGURE 12. For legend, see figure 9. Basic wave $D/\pi = 0.40$, $\epsilon/\pi = 0.05$. Perturbation is stable eigenvector. $P = 1$, $\epsilon/\pi = 0.005$.

D/π	Δ/π	S_R	S_i	Y_{crit}	Y_f	$(T_f)_{est}$	T_f
0.4	0.05	−0.2072	0.0107	−0.1914	−0.2486	69	94
0.5	0.04	−0.2259	0.0065	−0.1892	−0.2011	203	184
0.4	0.035	−0.2291	0.0053	−0.1792	−0.1908	308	236

TABLE 4. Estimated Y-level of filamentation Y_{crit} and filamentation time $(T_f)_{est}$ compared to calculated values, Y_f and T_f respectively for unstable waves of table 1. For all cases $P = 1$ and the perturbation is the unstable eigenvector with $\epsilon = \Delta/10$.

$T_f' = \omega t_f$, where T_f' is the time at which the wave just begins to overturn, and this occurs when the interface minimum Y_f takes the values shown.

We interpret these results, namely that the stable wave of figure 10 shows no growth in waveheight and no tendency towards filamentation but that it is seen in figures 11–12 and in the other cases tabulated in table 4 for the unstable waves, as evidence that, for the vortex equilibria given by the primary wave at arbitrarily small Δ and with perturbations at sufficiently small ϵ, the underlying cause of filamentation is the instability calculated in §3 and §5. If this speculation is correct we would expect filamentation of the vorticity interface for our wall-bounded vortex

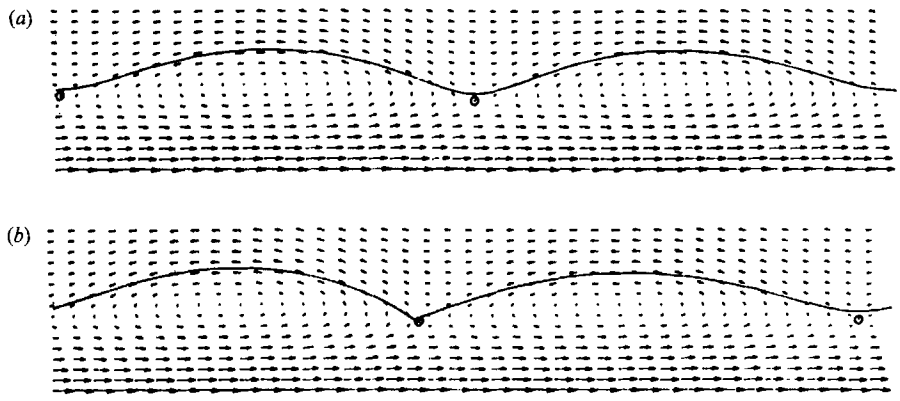

FIGURE 13. Velocity vector plot obtained in a reference frame moving with speed $U_{\rm rel}$ = (0.1775, 0) relative to the stationary fluid at $Y \to \infty$. $D/\pi = 0.40$, $\Delta/\pi = 0.05$. Perturbation is unstable eigenvector with $\epsilon/\pi = 0.005$. (*a*) $T = 0$, (*b*) $T = 95.28$. Note the presence of a hyperbolic stagnation point (⊙) positioned immediately below the interface minimum at $T = 0$ and very near the interface at the onset of filamentation when $T = 95.28$.

layer following disturbances to the parallel flow that are sufficiently close to a primary wave with wavelength in the range given by (5.6). We are not suggesting that filamentation is the occurrence of a singularity in the Euler equations but that it corresponds to the production of large but finite curvature at isolated points in the presence of an overturning interface.

Having identified a mechanism for the growth of interface perturbations, there remains the question concerning the kinematical cause of the interface overturning which results in filamentation. Some insight into this may be gained by an examination of the velocity field near the interface at times T near the onset of filamentation. Figure 13 shows velocity-vector plots, at times $T = 0$ and $T = 95.28$, in a frame of reference moving with X-velocity $U_{\rm rel} = 0.1775$ relative to the fluid at rest at $Y \to \infty$. In figure 14 we show a magnified view of the vector field at the point of filament formation. The frame of reference corresponding to $U_{\rm rel} = 0.1775$ was found by trial and error using the criterion that the interface minimum should be approximately stationary just at the beginning of filamentation. Note in figure 13 and more clearly in figure 14 the presence of a moving hyperbolic stagnation point which almost coincides with the interface extremum when filamentation begins. This is strong evidence that the actual process of filamentation for our class of initial disturbance is related to the presence of a stagnation point in the frame moving with the wave (see also Melander, McWilliams & Zabusky 1987). When the stagnation point touches the interface profile, the irrotational fluid above the interface crosses the dividing streamline (see for example figure 14*c*) and the subsequent interface distortion results in filamentation as is clearly seen in figures 14(*d*) and 14(*e*). This mechanism is then rather similar to the (axisymmetric) distortion of the boundary of the Hills spherical vortex by the rear stagnation point following a small boundary disturbance away from the spherical (Moffat & Moore 1979).

Our interpretation of the computations is that for our flow the stagnation point is not itself produced by the filamentation phenomenon. This is clear from figure 13(*a*) which shows stagnation points in the flow near the interface minimum at $T = 0$. These appear to be associated with the well-known 'cat's eye' streamline pattern which forms in a shear flow subject to wavelike motion. They will be present for primary waves of arbitrarily small Δ.

In the present context an estimate of the y-level of the stagnation point can easily be made. Assume for the flow depicted in figure 11 and figures 13–14, that the disturbance eigenvector can be approximated by a single mode with local wavelength equal to that associated with its dominant component $m = 1$ (table 2). With respect to the flow at rest as $y \to \infty$, this disturbance moves with speed

$$u_{\text{rel}} = \left(C + \frac{S_{\text{R}}}{P+2m}\right)\frac{\omega\lambda}{\pi}, \tag{6.2}$$

where $C = 0.2605$ is the main wave speed. Using $P = 1$, $m = 1$ and $S_{\text{R}} = -0.2072$ from table 2 gives $u_{\text{rel}} = 0.1914$ $(\omega\lambda\pi^{-1})$ compared to the dimensionless value of 0.1775 for the numerically measured speed of the reference frame, discussed earlier, in which the interface minimum is stationary at the point of filament formation. The agreement is sufficiently close to suggest that, to first order, the preferred frame of reference for viewing the kinematical events controlling filamentation is that moving with velocity given by (6.2). Now consider the Y-level of the critical layer (i.e. $u = 0$) of the basic flow in this reference frame. It is at this Y-level, to first order, where 'cat's eye'-type critical points will appear when the basic flow is disturbed by the presence of the primary wave plus the perturbation. From (6.2) this is $y_{\text{crit}} = -[C + S_{\text{R}}/(P+2m)]\,\lambda\pi^{-1} = -0.1914\lambda\pi^{-1}$. By comparison, the y-position of the interface at the point of filament formation, say in figure 14(*b*) is $y_{\text{f}} \approx -0.2486\lambda\pi^{-1}$. Estimates of Y_{crit} compared to the calculated Y_{f} for the other unstable waves of table 1 are given in table 4. While not perfect the agreement between Y_{crit} and Y_{f} is consistent (note that we have neglected the effect of the finite amplitude wave on Y_{crit}; the error is expected to be $O(\Delta)$) with the hypothesis that stagnation points producing filamentation arise in the perturbed critical layer of the shear flow.

An estimate of the time to filamentation $T_{\text{f}} = \omega t_{\text{f}}$ may now be made. Assuming that the interface has an initial minimum $Y = \bar{Y}_{\text{min}}$ corresponding to the primary wave (see table 1) and that the perturbation begins at the interface minimum and grows with the linear growth rate $S_{\text{I}}(\Delta, D, P)$ given by the spectral results, then T_{f} is the time for growth to Y_{crit}, and is given by

$$\bar{Y}_{\text{min}} - \epsilon \exp(S_{\text{I}} T_{\text{f}}) = Y_{\text{crit}}. \tag{6.3}$$

Our earlier estimate $Y_{\text{crit}} = -[C + S_{\text{R}}/(P+2m)]$ then gives

$$T_{\text{f}} = S_{\text{I}}^{-1} \log\left[\left(C + \frac{S_{\text{R}}}{P+2m} + \bar{Y}_{\text{min}}\right)\Big/\epsilon\right]. \tag{6.4}$$

Using $S_{\text{I}} = 0.01069$ (table 3), $\Delta/\pi = 0.05$, $\epsilon/\pi = 0.005$ and $\bar{Y}_{\text{min}} = -0.183584$ (table 1) gives $T_{\text{f}} = 69$ compared with $T_{\text{f}} \approx 94$ from figure 11. Estimates for the other unstable cases compared to the calculated ωt_{f} are shown in table 4. When $\Delta \to 0$, the spectral results show $f_1 \to 1$, i.e. $S_{\text{max}} \to \Delta^2$. Now when Δ is very small the difference between a pure cosinusoidal disturbance and a primary wave of the same amplitude Δ can be viewed as a perturbation with amplitude $\epsilon = O(\Delta^2)$. This is because the shape of the primary wave can be expressed as a power series in Δ. Hence for a pure cosinusoidal disturbance with wavelength in the spectrally unstable range, from (6.4) with $S_{\text{I}} = S_{\text{max}}$, our estimate for T_{f} is then

$$T_{\text{f}} = -\text{const}\,\Delta^{-2}\log\Delta, \tag{6.5}$$

which may be taken as the principal result of this paper.

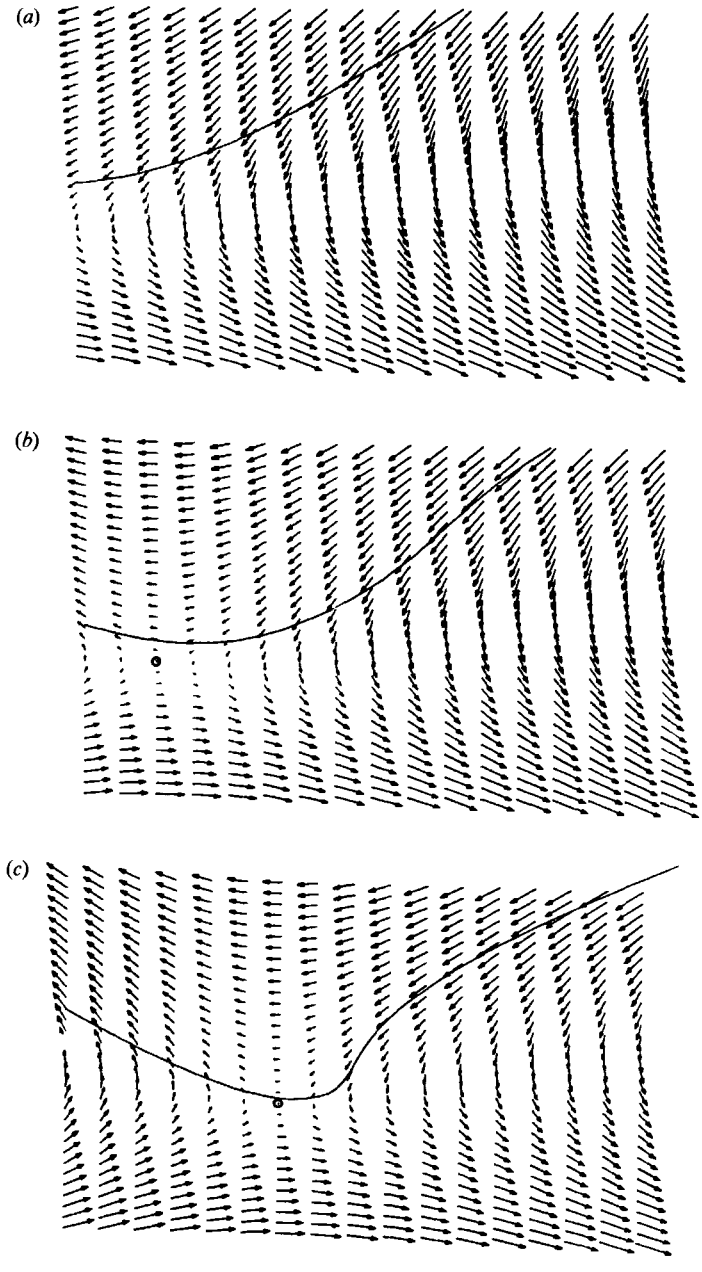

FIGURE 14 (*a*,*b*,*c*). For caption see facing page.

The limiting primary wave of maximum Δ occurs when the wave trough, or more precisely, the wave extremum on the rotational side of the interface just touches a hyperbolic critical point in the reference frame of the primary wave, and the interface forms a corner of angle $\frac{1}{2}\pi$ (Broadbent & Moore 1985; Pullin & Jacobs 1986). This may perhaps be viewed as a form of degenerate filamentation, although we stress again that filamentation does not require or imply the presence of a corner or cusp at the interface. A referee has pointed out that for this limiting wave, consistency requires that the speed of the perturbation relative to the primary wave should

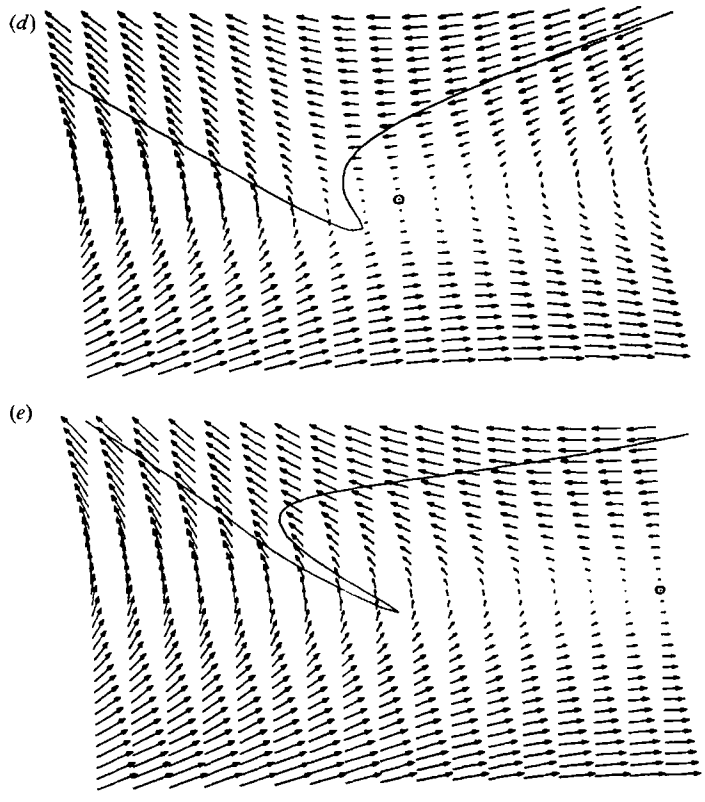

FIGURE 14. Magnified view of velocity vector plot near breaking interface. $U_{\text{rel}} = (0.1775, 0)$. Parameters as for figure 13. (*a*) $T = 91.66$, (*b*) $T = 92.87$, (*c*) $T = 94.08$, (*d*) $T = 95.28$, (*e*) $T = 96.49$. Note the presence of the moving hyperbolic stagnation ($\odot$) point near the breaking interface.

vanish, i.e. $S_{\text{R}} \to 0$. We find monotonic decrease in S_{R} when Δ increases from zero but for reasons discussed previously we have been unable to calculate stability near the limiting primary wave.

7. Discussion

Consider the space $\mathscr{F}$ of Fourier coefficients corresponding to all possible initial conditions for x-periodic or aperiodic (to include (5.1*a*) and (5.2*a*)) single-valued disturbances to our basic flow with mean depth of shear layer d. The primary waves are fixed points in $\mathscr{F}$ lying on families of curves in $\mathscr{F}$ with parameters δ and d. For given d there is a curve with parameter δ which runs continuously (apart from possible bifurcations which have not been investigated) from the origin to a point in $\mathscr{F}$ corresponding to the limiting wave for that d, where the wave crest meets a hyperbolic critical point in the reference frame moving with the primary wave. Fixed points are either stable or unstable to infinitesimal subharmonic perturbations dependent on d/λ as given by (5.6). In D1 it is hypothesized that almost all perturbations (our sense) to vortex equilibria will filament in a time inversely proportional to the square of the amplitude of the perturbation by nonlinear focusing to smaller scales. The evidence refers to isolated perturbations to stable Kirchoff elliptical vortices including the circular vortex patch as a special case, and relies on identification of filamentation with breakdown of a weakly nonlinear approximation

to the full CD equations. In the present context this implies that all points in $\mathscr{F}$ including points arbitrarily close to either a stable or unstable fixed point will filament in time proportional to ϵ^{-2} by nonlinear focusing to smaller scales, where ϵ may be taken as some measure of the distance in $\mathscr{F}$ to the nearest fixed point.

Our conclusions are more restricted and can be summarized as follows:

(i) One possible mechanism of filamentation is the instability of primary waves (fixed points) of finite or of arbitrarily small amplitude to infinitesimal subharmonic perturbations. We note that primary waves have a dominant Fourier mode.

(ii) In this case the mechanism of filamentation is the approach of the wave extremum to a hyperbolic critical point at or near the critical layer of the primary wave in a reference frame defined by the perturbation.

(iii) The time for filamentation when the primary wave is unstable is given by (6.5) and scales inversely on the square of the amplitude of the disturbance.

(iv) Any disturbance will filament immediately if it contains a dominant Fourier mode with coefficient a and wavenumber k such that ka exceeds 0.5, since this places the wave extremum at a critical layer associated with the dominant mode.

There then appear to be three mechanisms of filamentation for a point in $\mathscr{F}$. First is the response to a large perturbation (iv), which may be viewed as a sufficient but not necessary condition for filamentation. This essentially kinematic event accounts for the filamentation seen by Pullin (1981) and by Stern (1985). We shall refer to this as the kinematic mechanism. Second is the linear-instability of the primary wave (i)–(iii). This includes our calculations and the Polvani, Flierl & Zabusky (1989) instability of the Kirchoff elliptical vortex with aspect ratio $a/b > 3$. Our case is interesting in that the primary wave may be of arbitrarily small amplitude and close to the basic flow whereas for the vortex patch the amplitude of the primary wave (viewing the circular patch as the basic flow) has to be large. Thirdly is the nonlinear-cascade mechanism proposed by D1. It is clear that this is distinct from the linear-instability mechanism since the numerical evidence indicates that filamentation can occur without growth in waveheight: the linear-instability mechanism produces waveheight growth towards critical points of the velocity field which are present by virtue of the finite amplitude primary wave, while for the D1 mechanism, a steepening is produced by weakly-nonlinear interactions, which then produce a critical point at the interface and filamentation follows.

According to these arguments it is then possible that our primary waves may filament in time $O(\epsilon^{-2})$ by the D1 mechanism irrespective of spectral stability in the sense of §5, although we stress that there is, as yet, no hard evidence for this. For the case of a pure cosinusoidal disturbance to the basic flow with arbitrarily small amplitude Δ, then since $\epsilon = O(\Delta^2)$ as previously argued, it follows that T_f would then be $O(\Delta^{-4})$, which would be very difficult to verify by purely numerical means when $\Delta \to 0$. For spectrally unstable primary waves this is longer than $\Delta^{-2}\log(\Delta)$ as given by (6.5) so we would expect the linear-instability mechanism to be dominant in these circumstances.

Having analysed the linear-instability mechanism in §6 we now distinguish between the kinematic and the D1 nonlinear-focusing mechanisms by a particular example. We follow D1 and consider an almost-isolated antisymmetrical disturbance to a deep shear layer ($d \to \infty$) of the form

$$Y(X,0) = A\left(\frac{X}{X_0}\right)\exp\left(-0.5\left(\frac{X}{X_0}\right)^2\right) \quad (-\pi < X < \pi), \tag{7.1}$$

N	A	Δ_0	T_f
400	1/10	0.3032	3.1
400	1/20	0.1516	24.0
400	1/40	0.0758	175.9
850	$\sqrt{2}/80$	0.0536	351.8
400	$-1/20$	-0.1516	66.0
850	$-\sqrt{2}/80$	-0.0536	449.1

TABLE 5. Filamentation time T_f for antisymmetric almost isolated disturbance, equation (7.1). All cases have $m = 20$.

repeating every 2π in the X-direction, so that the flow is X-periodic. In (7.1) $X_0 = \pi/m$ and $\delta = A\exp(-0.5)$ is the waveheight. The local wavelength may be taken as $\lambda = 4X_0$ and so the equivalent amplitude $\Delta_e = \delta\pi/\lambda = 0.156Am$. Since (7.1) is not near a primary wave in $\mathscr{F}$ (we know of no solitary-wave-like fixed points which would resemble (7.1) when $A \to 0$ and we doubt their existence) then the basic flow should be viewed as the vortex equilibrium state, so that (7.1) means our sense of both disturbance and perturbation. Seven CD calculations were performed each with $m = 20$ but with differing values of A and N listed in table 5, which also shows the observed time T_f to filamentation for each case. The results for $A > 0$ may be consistent with the asymptotic scaling $T_f = O(\Delta_e^{-2})$ suggested in D1. For the case with $A = \frac{1}{20}$, the initial disturbance is the negative of case 30 in D1, which is equivalent to putting $A = -\frac{1}{20}$ in (7.1). This has the puzzling effect of increasing T_f from $T_f = 24$ ($A = \frac{1}{20}$) to $T_f = 66$ ($A = -\frac{1}{20}$)? When $A = \pm\sqrt{2}/80$ the effect on T_f of sign (A) is much reduced but remains of order several wave periods. This suggests that smaller A than used presently may be required to determine the true asymptotic behaviour of T_f when $A \to 0$.

In figure 15 we illustrate filamentation with $A = \frac{1}{10}$ ($k\delta = 0.6064$). This occurs immediately by the kinematic mechanism with the interface overturning intrusively at the trailing depression. We found that a purely cosinusoidal disturbance with $\Delta = 0.3032$ (not shown) exhibited locally similar filamentation at the same T_f. By contrast, in figure 16 with $A = \frac{1}{40}$, there is local steepening as found in D1 at the leading edge of the disturbance (the local phase velocity of the disturbance extrema is from left to right) which produces intrusive filamentation at $T_f = 176$ presumably by the D1 mechanism. The different interface geometry is characteristic of the different mechanisms: that for the kinematic mechanism is of course locally similar to filamentation by the linear-instability mechanism (e.g. figure 11) but no interface growth dynamics are required.

Finally we remark that all cases of filamentation observed here for the parallel basic flow with irrotational flow on one side of the interface exhibit intrusive filamentation whilst that seen in D1 for vortex patches in plane flow (with the exception of case 30) and by Polvani, Flierl & Zabusky (1988) show extrusive filamentation in the sense that the filament grows into the irrotational fluid surrounding the vortex patch. For the kinematic and the linear-instability mechanism this can be explained from the fact that, in the reference frame that rotates with the Kirchoff ellipse there is effective shear exterior to the interface which then places the relevant critical points of the vortex equilibria in this domain. This

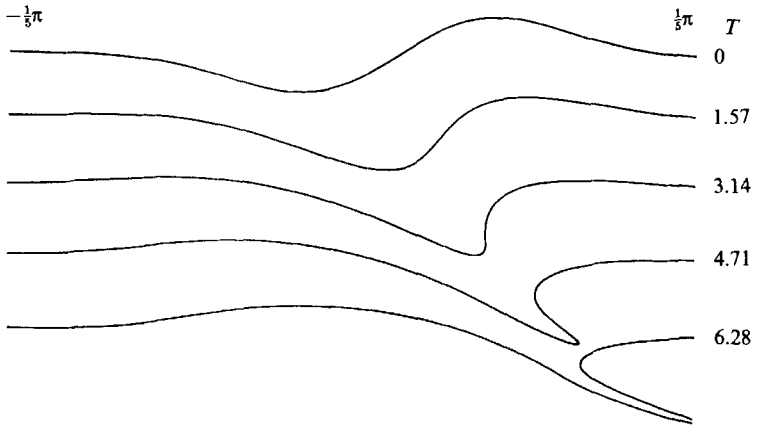

FIGURE 15. Evolution of portion of wave profile in $-\frac{1}{5}\pi < X < \frac{1}{5}\pi$ with antisymmetric almost isolated initial disturbance (7.1). $A = \frac{1}{10}$, $m = 20$. Flow above interface is irrotational and flow below has unit vorticity.

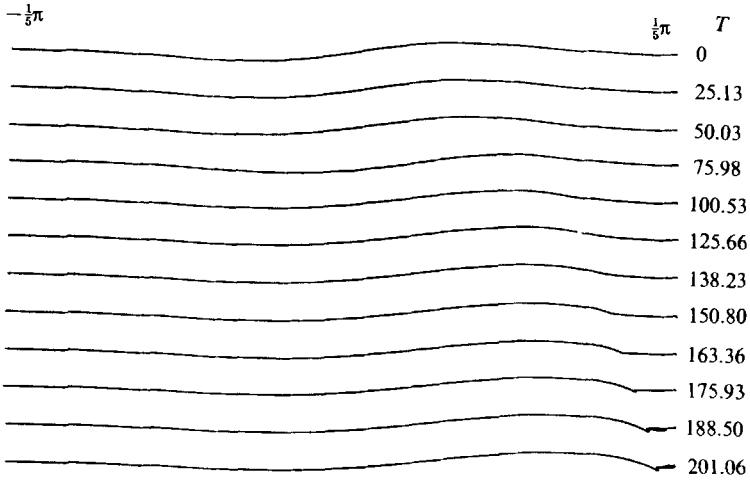

FIGURE 16. For legend, see figure 15. $A = \frac{1}{40}$, $m = 20$.

can be demonstrated as follows: consider a uniform circular vortex of radius $r = r_0$ and vorticity ω. When subject to perimeter shape disturbances of the form

$$r = r_0 + \delta \exp[\mathrm{i}(M\theta - \sigma_M t)], \tag{7.2}$$

where θ is a polar angle, $\delta \ll r_0$ and M is integral, then to $O(\delta)$, the wave crests move with angular velocity (Lamb 1932, §158)

$$\frac{\sigma_M}{M} = \frac{(M-1)}{M}\tfrac{1}{2}\omega. \tag{7.3}$$

If we move in a frame of reference rotating with this angular velocity, then the tangential velocity distribution for the mean flow is

$$v_\theta = \frac{\omega r}{2M} \quad (r \leqslant r_0), \tag{7.4a}$$

$$v_\theta = \tfrac{1}{2}\omega\left[\frac{r_0^2}{r} - \left(1 - \frac{1}{M}\right)r\right] \quad (r > r_0). \tag{7.4b}$$

In this reference frame the flow is rotational in $r > r_0$. There is thus an effective critical layer, where $v_\theta = 0$, at $r = r_c$, where from (7.4*b*)

$$r_c = r_0\left(\frac{M}{M-1}\right)^{\frac{1}{2}}.$$

In our rotating frame of reference in which to $O(\delta)$, the wave crests are stationary, there will exist hyperbolic critical points in the presence of the wave at $r \approx r_c$, $\theta = 2(m-1)\pi/M$, $m = 1, \ldots, M$ on the true irrotational side of the interface. The Kirchoff ellipse has $M = 2$.

For the D1 nonlinear-cascade mechanism following small isolated disturbances to the circular patch, filamentation appears intrusive when viewed in the reference frame of the vortex patch solid-body rotation but we can find no obvious explanation. This and other questions concerning, for example, the detailed nature of the D1 mechanism and the possibility of spontaneous corner formation in vorticity-interface evolution must await further research.

The comments and criticisms of Dr David Dritschel on several versions of this paper are gratefully acknowledged. This work was supported by the Australian Research Council under grant number A48315031.

REFERENCES

Balagondar, P. M., Maslowe, S. A. & Melkonian, S. 1987 The propagation of finite-amplitude waves in a model boundary layer. *Stud. Appl. Maths* **76**, 169–185.

Benney, D. J. & Maslowe, S. A. 1975 The evolution in space and time of nonlinear waves in parallel shear flows. *Stud. Appl. Maths* **3**, 181–205.

Berk, H. L., Neilsen, C. E. & Roberts, K. V. 1970 Phase space hydrodynamics of equivalent nonlinear systems; experimental and computational observations. *Phys. Fluids* **13**, 980–995.

Broadbent, E. G. & Moore, D. W. 1985 Waves of extreme form on a layer of uniform vorticity. *Phys. Fluids* **28**, 1561–1563.

Deem, G. S. & Zabusky, N. J. 1978*a* Vortex states: stationary V-states, interactions, recurrence, and breaking. *Phys. Rev. Lett.* **40**, 859–862.

Deem, G. S. & Zabusky, N. J. 1978*b* Stationary V-states, intereactions, recurrence and breaking. In *Solitons in Action* (ed. K. Langer & A. Scott), pp. 277–293. Academic Press.

Dritschel, D. G. 1988*a* The repeated filamentation of two-dimensional vorticity interfaces. *J. Fluid Mech.* **194**, 511–547.

Dritschel, D. G. 1988*b* Contour surgery: a topological reconnection scheme for extended integrations using contour dynamics. *J. Comp. Phys.* **77**, 240–266.

Jacobs, P. A. & Pullin, D. I. 1985 Coalescence of stretching vortices. *Phys. Fluids* **28**, 1619–1625.

Lamb, H. 1932 *Hydrodynamics*, 6th edn. Cambridge University Press.

McLean, J. W. 1982 Instability of finite amplitude water waves. *J. Fluid Mech.* **144**, 315–330.

McLean, J. W., Ma, Y. C., Martin, D. U., Saffman, P. G. & Yuen, H. C. 1981 Three-dimensional instability of finite-amplitude water-waves. *Phys. Rev. Lett.* **46**, 817–820.

Melander, M. V., McWilliams, J. C. & Zabusky, N. J. 1987 Axisymmetrization and vorticity gradient intensification of an isolated two-dimensional vortex through filamentation. *J. Fluid Mech.* **178**, 137–139.

Moffatt, H. K. & Moore, D. W. 1979 The response of Hill's spherical vortex to a small axisymmetric disturbance. *J. Fluid Mech.* **87**, 749–760.

Polvani, L. M., Flierl, G. R. & Zabusky, N. J. 1989 The filamentation of unstable vortex structures via separatrix crossing: a quantitative estimate of onset time. *Phys. Fluids* A **1**, 181–184.

Pullin, D. I. 1981 The nonlinear behaviour of a constant vorticity layer at a wall. *J. Fluid Mech.* **108**, 401–421.

Pullin, D. I. & Grimshaw, R. H. J. 1986 Stability of finite-amplitude interfacial waves. Part 3. The effect of basic current shear for one-dimensional instabilities. *J. Fluid Mech.* **172**, 277–306.

Pullin, D. I. & Jacobs, P. A. 1986 Nonlinear waves in a shear flow with a vorticity discontinuity. *Stud. Appl. Maths* **75**, 77–94.

Rayleigh, Lord 1880 *Scientific Papers*, vol. 1, pp. 474–487. Also *Proc. Lond. Math. Soc.* **11**, 57–80.

Rayleigh, Lord 1887 *Scientific Papers*, vol. 3, pp. 17–23. Also *Proc. Lond. Math. Soc.* **19**, 67–74.

Roberts, K. V. & Christiansen, J. P. 1972 Topics in computational fluid mechanics. *Comput. Phys. Commun. Suppl.* **3**, 14–32.

Stern, M. E. 1985 Lateral wave breaking and shingle formation in large-scale shear flow. *J. Phys. Oceanogr.* **15**, 1274–1283.

Stern, M. E. & Pratt, L. J. 1985 Dynamics of vorticity fronts. *J. Fluid Mech.* **161**, 513–532.

Zabusky, N. J., Hughes, M. H. & Roberts, K. V. 1979 Contour dynamics for the Euler equations in two dimensions. *J. Comp. Phys.* **30**, 96–106.